

Ultra-wideband Transmissive Linear Polarization Device Based on Graphene

Liwei Guo¹, Simin Li^{1,2,*}, Xing Jiang¹, Xin Liao¹, and Lin Peng¹

¹ School of Information and Communication
Guilin University of Electronic Technology, Guilin 541004, China

² School of Electrical and Information Engineering
Guangxi University of Science and Technology, Liuzhou 545006, China
siminl_guet@163.com

Abstract — In order to achieve both adjustable wideband and high Polarization Conversion Rate (PCR) of the transmitted waves, a novelty tri-layered structure is proposed for terahertz applications. The Rhombus Hollow Square (RHS) is built up by top and bottom gold gratings on Silicon Dioxide and Polyamide substrate with graphene strips. The proposed polarizer broadens the bandwidth and has well performance. As chemical potential increases, the bandwidth is also broadened by adjusting the graphene. From 0.5 THz to 3 THz, the PCR is greater than 90%, and the relative bandwidth up to 142.9%. The transmission and absorption of polarizer are analyzed at the oblique incidence with chemical potential 0.1eV. By simulating and analyzing the performance, a new result of maintaining broadband and high transmittance in oblique incidence is obtained.

Index Terms — Graphene, Terahertz, transmitting polarizer, ultra-wideband.

I. INTRODUCTION

Usually, terahertz (THz) wave is a length of 3000 to 30 μm , and the frequency is 0.1 to 10 THz. The application of terahertz technology in the field of electromagnetics is a hot topic now [1-2]. Terahertz is used in fields such as high-temperature superconducting materials, semiconductor materials properties research, and broadband communication [3], microwave device [4-6] and so on. Currently, there are mainly three types of polarizers used in the terahertz band liquid crystal polarizers [7], carbon nanotube polarizers [8], and metal wire grid polarizers [9]. Metal wire grid polarizers can be obtained mainly through precision machining, laser direct writing technology, photolithography and other processing methods. This is also the most widely used terahertz polarizer.

Generally, metal is fine material to design metamaterials and which is designed for reflective [10-12] and transmitting polarization converters [13-18]. For some non-adjustable materials, such as dielectric

materials and metal materials, which dynamic control becomes more inconvenient, and its application is limited. However, there are many advanced technologies for terahertz/mid-infrared tunable polarizer. In particular, the transmittance of the polarization control is adjustable. The bandwidth is broadened by adjusting the parameters of graphene to design the structure. This research provides a unique idea for the controllable polarization conversion rate in the research [18].

At the same time, the graphene has high electron mobility, the electrical grating or doping level of graphene can be adjusted to make it conductive [19-30]. For example, the absorbers [19] are tunable graphene based with polarization insensitive [20]. Light efficiently into graphene surface plasmon can be captured by the graphene sheet [21]. The graphene frequency selective surface achieves tunable polarization rotation of the transmitted wave and controllable bandpass response [23]. Graphene can be combined with other materials, which performance and bandwidth will enhance [24].

The conductivity of graphene is used to control by voltage [25]. According to design the polarization converter, the electron scattering time characteristic of graphene ranges from *ps* to *sub-ps*, which can vary in a wide range of frequency. MMW/IR beam synthesizer based on graphene infrared window, used for MMW/IR compound Compact Antenna Test Range (CATR), solves the infrared transmittance in the MMW/IR compound target simulation system [26].

We propose an original cross-polarized tri-layered structure metamaterial converter, which is a new transmission type, based on graphene to optimize the conversion rate and widened the operating frequency. We validated transmitting rate and high polarization conversion rate by full-wave numerical simulations. The physical mechanisms of the device are also discussed.

II. DESIGN OF TRANSMITTING POLARIZER BASED ON GRAPHENE

A schematic diagram of the unit structure of a

metamaterial cross-polarized transmission converter based on graphene strip, in which a vertically incident x -polarized waves are transformed to cross-polarized waves. The RHS patch, which arranged at a diagonal of 45° in Fig. 1 (a). The dielectric spacers are silicon dioxide and polyamide, with the RHS and graphene strip between them. The top and bottom of the polarizer are gratings. The gold grating wire width and periodicity both are w , and the thickness of the grating is $0.1\mu\text{m}$. The gratings are respectively covered on the substrates.

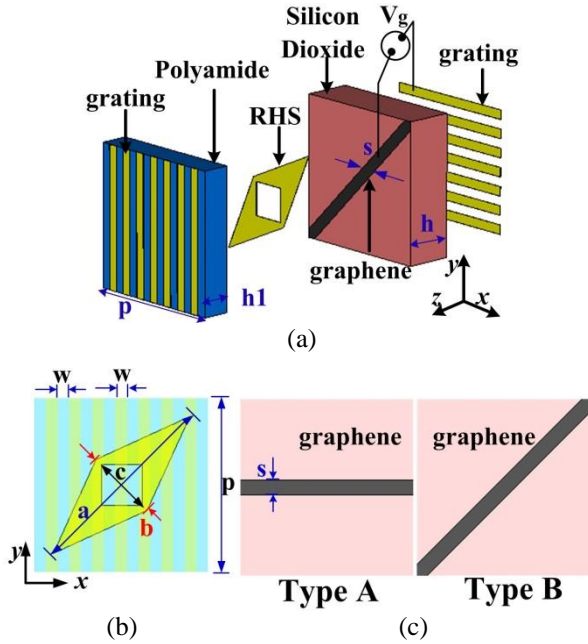


Fig. 1. (a) Schematic and geometric dimensions of transmissive polarizer unit cell by graphene, (b) the RHS of polarizer, and (c) type of the graphene strips in the structure.

The middle part of the transmitting polarizer is composed of graphene strip and a metal resonator layer RHS in Fig. 1 (b), which is located on the bottom $20\mu\text{m}$ -thick substrates. The unit is arranged in a periodic array structure of constant p . The structural parameters of the graphene strips are p and s , respectively. The two types of graphene strips are along the x -axis and rotated 45 degree with the unit diagonally, respectively. The thickness of the graphene strips and RHS are 100 nm . And the tri-layered structure substrate uses Silicon Dioxide thickness of h and Polyamide thickness of h_1 respectively. Table 1 shows the optimized parameters of the structure. In order to excite the metal resonator RHS, the polarization field is applied along the $-z$ -direction when the terahertz waves are normally incident. Simultaneously, graphene strips are located under the RHS transmitting polarizer to proactively modulate the near-field coupling effect of terahertz waves.

Table 1: The optimal parameters of the polarizer

Parameters	p	c	s	b	w	h	h_1	a
Value(μm)	60	20	5	25	4	20	12	67

In the research, the structures were numerically investigated through frequency domain solver by CST Studio Suite 2020 of commercially available full-wave electromagnetic simulator software. The unit calculation is shown in the Fig. 2. The periodic boundary structure is unit cell and floquet ports on the top and bottom. In the terahertz band, the three-layer metal-graphene-metal layers realize the controllable characteristics of linear transmission and perfect polarization conversion.

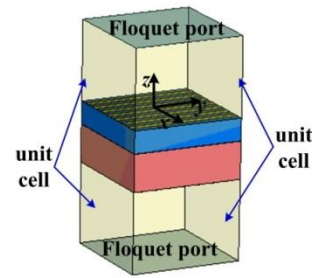


Fig. 2. The model of numerically investigates.

Two polarizers in the form of graphene are analyzed. Type A is a horizontal graphene strip and Type B which graphene with 45° angle in the horizontal direction. The graphene layer is shown in Fig. 1 (c), which is isolated by Silicon Dioxide with a dielectric constant $\epsilon_r=3.9$ and Polyamide with a dielectric constant of 3.5 . Introduce the conductivity of the graphene strip according to the Kubo formula, which is mainly intra/inter-band [27]:

$$\sigma_s = \sigma_{intra}(\omega, \mu_c, \Gamma, T) + \sigma_{inter}(\omega, \mu_c, \Gamma, T), \quad (1)$$

$$\sigma_{intra}(\omega, \mu_c, \Gamma, T) = \frac{-je^2kBT}{\pi\hbar^2(\omega - j2\Gamma)} \left(\frac{\mu_c}{kBT} + 2\ln(e^{-\mu_c/kBT} + 1) \right), \quad (2)$$

$$\sigma_{inter}(\omega, \mu_c, \Gamma, T) = -j \frac{e^2}{4\pi\hbar} \ln \left(\frac{2|\mu_c| - (\omega - j2\Gamma)\hbar}{2|\mu_c| + (\omega - j2\Gamma)\hbar} \right), \quad (3)$$

where the kB and T represent Boltzmann's constant and temperature. Parameters e and σ are the electron charge and Planck's constant, respectively. In addition, τ and μ_c refer to the relaxation time and chemical potential, namely Fermi energy E_F . The $\tau=1\text{ps}$, meanwhile $T=300\text{K}$. Therefore, $\sigma=1/2\tau$ represents the frequency of collision.

Before analyzing the design, it is necessary to consider the selectivity structure of the polarizer. In the first design, use graphene strips instead of whole graphene sheets. Then, the polarization of the transmitted wave with the applied voltage between the graphene strip and the gold grating is investigated. The permittivity of graphene [2] can be obtained by $\epsilon = 1 + (i\delta_s)/(\epsilon_0\omega\Delta t)$ in

the CST Studio Suite 2020. The carrier density and the position of the μ_c among the strips can be restrained with the bias voltage, and the phenomenon is dynamically. Formula (4) gives an approximate expression related to μ_c and V_g :

$$E_F = \mu_c \approx \hbar v_f \sqrt{\frac{\pi \epsilon_r \epsilon_0 V_g}{et}}, \quad (4)$$

The parameters ϵ_0 and ϵ_r respectively represent the dielectric constant of vacuum and silicon dioxide. The parameter V_g is bias voltage. The parameters e and V_f are the electronic charge and the Fermi velocity at 1.1×10^6 m/s in graphene, respectively. The $t=20$ nm is the thickness of the insulating layer between the graphene and the electrode. Novel polarizer we designed, the maximum bias voltage of 100V is adopted. Calculated by the formula, as the external load voltage increases, the chemical formula gradually increases. The adjustment range of the E_F is between 0eV-1eV, which requires range 5V to 75V bias voltage.

III. SIMULATION RESULTS AND DISCUSSIONS

The original unit structure of we proposed in Fig. 1 with the Cartesian coordinates of x - y - z axis. The periodic unit can be designed as a polarizer. If the incident and transmitted wave are E^i and E^t , respectively. The both forward and backward propagation of the transmission polarizer can be used as a four-port transmission system with the two ends as input and output. Then the positive propagation and opposite propagation can be indicated as the equation of electric field [28].

The superscript p indicate positive propagation along the $-z$ direction of forward, and the o indicate opposite propagation along the $+z$ of backward:

$$\begin{cases} \vec{E}^i = \begin{pmatrix} E_x^i \hat{x} \\ E_y^i \hat{y} \end{pmatrix} e^{jkz} \\ \vec{E}^t = \begin{pmatrix} E_x^t \hat{x} \\ E_y^t \hat{y} \end{pmatrix} e^{jkz} \end{cases}, \quad (5)$$

$$\begin{pmatrix} E_x^{io} \\ E_y^{io} \\ E_x^{ip} \\ E_y^{ip} \end{pmatrix} \cdot T = \begin{pmatrix} E_x^{ro} & E_x^{rp} \\ E_y^{ro} & E_y^{rp} \\ E_x^{ro} & E_x^{rp} \\ E_y^{ro} & E_y^{rp} \end{pmatrix}. \quad (6)$$

In that way, the transmission coefficients and reflection coefficients of the positive (forward) and opposite (backward) propagation in two componential arrays are expressed by the 4×4 scattering matrix as:

$$T = \begin{pmatrix} t_{xx}^o & t_{xy}^o & t_{xx}^p & t_{xy}^p \\ t_{yx}^o & t_{yy}^o & t_{yx}^p & t_{yy}^p \\ t_{xx}^o & t_{xy}^o & t_{xx}^p & t_{xy}^p \\ t_{yx}^o & t_{yy}^o & t_{yx}^p & t_{yy}^p \end{pmatrix}. \quad (7)$$

The subscripts x and y denote the electromagnetic waves state of polarization, meanwhile mark down i and t denote incident and transmit terahertz waves respectively. The t_{yx} indicate y -polarization transmitting from x -polarization incidence. The r_{xx} indicate x -polarization co-polarized reflection amplitude from x -polarization incidence. We propose a transmitting metamaterial linear polarizer, which transform the incident x -polarized terahertz wave to y -polarized, which is pure cross-polarized wave. The Stokes method is introduced to accurately describe transmitted waves. Four parameters with the same physical dimensions are used to determine the polarization state:

$$Tr_{-0} = t_{xx}^2 + t_{yx}^2, \quad (8)$$

$$Tr_{-1} = t_{xx}^2 - t_{yx}^2, \quad (9)$$

$$Tr_{-2} = 2t_{xx}t_{yx} \cos \Delta\varphi, \quad (10)$$

$$Tr_{-3} = 2t_{xx}t_{yx} \sin \Delta\varphi. \quad (11)$$

The formula $\Delta\varphi = \phi_{yx} - \phi_{xx} = \arg(t_{yx}) - \arg(t_{xx})$ is the difference of phase between the cross-polarized transmission coefficient t_{yx} and opposite propagation coefficient t_{xx}^o . The polarization conversion rate (PCR) of a tunable transmitting polarizer is usually expressed in terms of conversion efficiency. The calculation formula is:

$$PCR = t_{yx}^2 / (t_{yx}^2 + t_{xx}^2). \quad (12)$$

Since electromagnetic energy may be lost, the absorption rate of the conversion rate is calculated. The absorption rate of transmission (A_t) designs formula:

$$A_t = 1 - t_{yx}^2 - r_{xx}^2. \quad (13)$$

The graphene-based transmitting polarizer is designed to perform linear polarization conversion in the transmitting mode, so the metal layer of the traditional reflective polarizer is replaced by gratings. The double-layered grating is shown in Fig. 1 (a). The tri-layered structure shown plays an important role in transmitting pure linear polarized waves. With the double-layer orthogonal metal gratings design, the upper grating layer will not block the incident wave, and the cross-polarized waves can be transmitted by bottom gratings, which reflect the co-polarized waves as the metal layer. In this way, a pure cross-polarized wave can be transmitted, while its reflection is prohibited, and the polarization conversion is improved.

In addition, vertical gratings are added in front of the RHS. The cross-polarized and the co-polarized transmittance obtained by numerical simulations and the phase difference with the x -polarization normal incidence are shown in Fig. 3. The transmission simulation result of the Type-A graphene polarizer is shown in Fig. 3 (a). The plots give information about the condition of loading 0dB incident power, the transmitted cross-polarized wave exceeds -3dB, which is equivalent to half of the energy transmitted. The opposite propagation t_{xx}^o can be

lower than -10dB from 1.25 THz to 2.0 THz. Between 2.0 THz and 2.7 THz, the decrease of the cross-polarization transmittance is due to the sharp increase of the opposite propagation. The co-polarization transmission t_{xx} (or t_{yy}) and t_{xy} are all below -30dB.

The Fig. 3 (b) plots the performance of another device Type B. Among 1.125 THz and 2.375 THz, the power of cross-polarization transmission exceeds -3dB, and from 2.0 THz to 2.375 THz, it exceeds -1dB. The opposite propagation t_{xx}^o in the same frequency band is less than -10dB, at some frequency points close to -20dB. It shows that the transmission mode linear polarization converter of Type B has a high-performance over a broad-band.

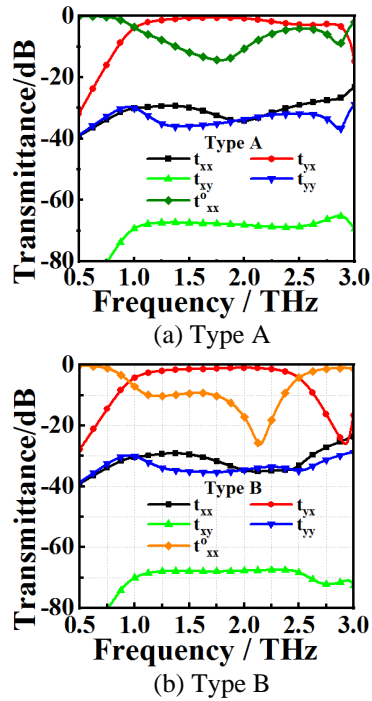


Fig. 3. Cross-polarized transmittance t_{yx} and opposite propagation t_{xx}^o are obtained through numerical simulations with x -polarization normal incidence. (a) Type A of graphene layout, and (b) Type B of graphene layout.

As shown in Fig. 4. (a), the PCR and the Absorption with x -polarized at normal incidence. First, we analyze the conversion rate of the Type A device. Between 0.5 THz and 2.75 THz the absorption ratio is kept below 20%. Between 0.75 THz and 2.8 THz the PCR is above 90%. In comparison, the performance of the Type B polarizer is analyzed in Fig. 4 (b). Between 0.5 THz and 2.75 THz the PCR is greater than 90%. At 2.9 THz, the PCR sudden decrease is due to the increase in opposite propagation t_{xx}^o and absorption of metasurfaces. The

parameter phase difference $\Delta\phi$ demonstrates the ability to transform the linear incoming wave by 90° of polarization. The absorption ratio of Type B decreases with the change of the chemical potential.

By comparison from Fig. 3 and Fig. 4, the Type B polarizer has better performance than the Type A. The device of Type B has a high-performance of 90% over a broad-band. Next, the performance of the graphene-loaded Type B polarizer was analyzed in detail.

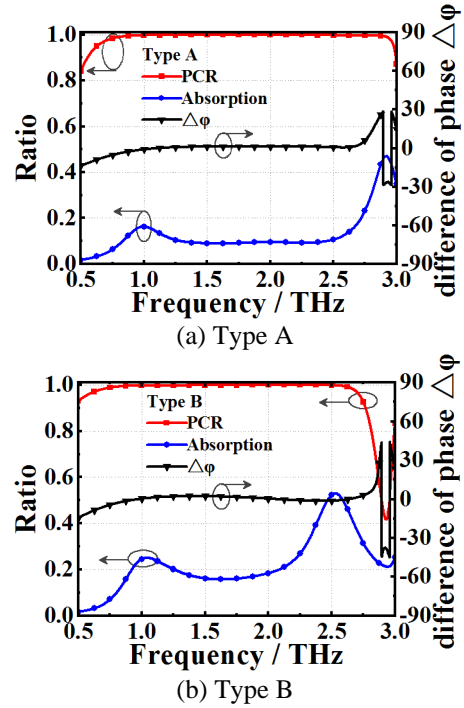


Fig. 4. The PCR and the Absorption and the phase difference with x -polarized normal incidence. (a) Type A of graphene layout, and (b) Type B of graphene layout.

IV. PERFORMANCE ANALYSIS

The principle of graphene-based double-layer transmission polarizer is F-P-like cavity. The schematic diagram of F-P-like cavity is shown in Fig. 5. In the multi-transmission process, the interference of polarization couplings may change total transmitted field about cross- and co-polarized. Analyze the interference process of waves to obtain the calculation method of transmittance. According to the formula definition, t_{xy}^h (r_{xy}^h) represent the y -polarized transmission (or reflection) coefficient of x -polarized incident on the h interface. The parameter h is 1 and 2, which represent the top and bottom of the F-P cavity, respectively. It should be noted that the transmittance (or reflectance) defined is equal to its square root, and it has nothing to do with the refractive index of the dielectric material near the interfaces.

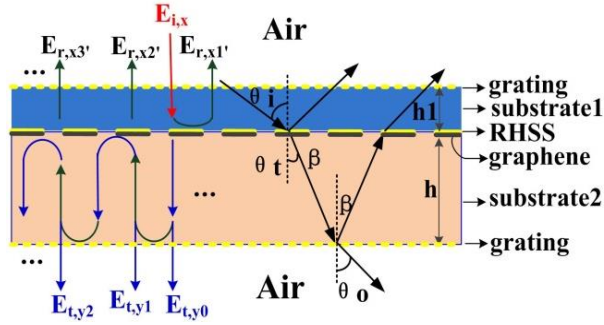


Fig. 5. Schematic diagram of a graphene-based double-layer dielectric F-P-like cavity.

According to the definition of light vector field in electromagnetic theory, the normal incident wave of x -polarized and the transmitted wave of y -polarized are $E_{i,x}$ and $E_{t,y}$. The letter n refers to the sequence round trip in the cavity. Generally, the grating layer is considered an ideal polarizer, and it can be easily calculated. Therefore, the y -polarized transmitting phase will be calculated, which ideal state is marked with a red line via Fig. 5. Under ideal conditions, since the y -polarized wave is transmitted round trip between the double-layer gratings, the electric field after the n th round trip is E_m , and the polarization transmission usually consists of several parts. Therefore, $E_{m,ym}$ ($m = 1, 2, \dots, 2n$) is defined to explain each transmission part of $E_{m,y}$. The amplitude of $E_{m,ym}$ decreases exponentially with the increase of n . The loss caused by the absorbing of the structure is directly proportional to n . From the above analysis, the transmitting energy will be acquired via superimposing principal of n terms, formula is:

$$\vec{E}_{t,n} \approx \vec{E}_{t,y1} + \vec{E}_{t1,y2} + \vec{E}_{t2,y3} + \vec{E}_{t3,y4}. \quad (14)$$

Next, the principle of the polarizer is discussed from the electric field and surface current, which are shown in Fig. 5 and Fig. 6 at 1.47THz, 1.95 THz, and 2.6 THz when $E_F = \mu_c = 0.1\text{eV}$. It is important to establish the electromagnetic coupling effect between the multilayer transmitting polarizer in detail from the physical principle of the F-P-like cavity.

While the terahertz wave is incoming the polarizer, Fig. 6 (a) and Fig. 6 (b) show the surface currents on the patch and graphene strip, respectively, where the chemical potential $E_F = 0.1\text{eV}$ at 1.95 THz. The surface current along the RHS in Fig. 6 (a) is the same as the induced current on the graphene strips in Fig. 6 (b) at 1.47 THz, 1.95 THz and 2.6 THz. The graphs show that the surface current is mainly distributed on the RHS patch. At 1.47 THz and 2.6 THz, the surface current and RHS are vertically downward and upward respectively. At 1.95 THz, the surface current is downward in the RHS direction. The direction of the surface current is different at different frequencies, so the equivalent wavelength is different.

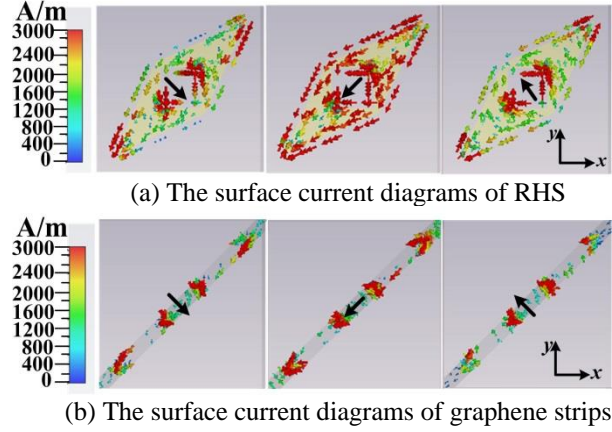


Fig. 6. The surface current diagrams of RHS and graphene strips at 1.47THz (left) 1.95 THz (middle) and 2.6 THz (right) when $E_F = \mu_c = 0.1\text{eV}$.

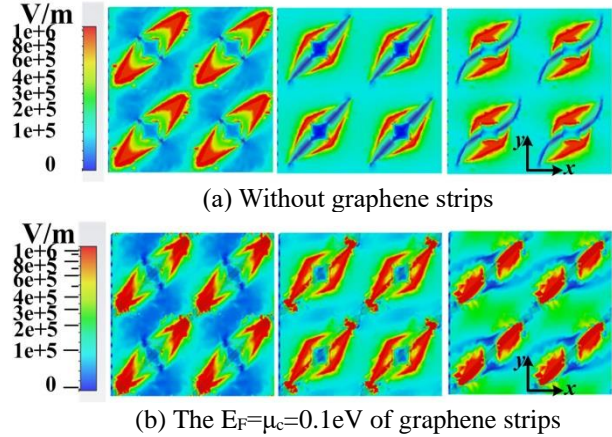


Fig. 7. The electric field diagrams of polarizer at 1.47THz (left) 1.95 THz (middle) and 2.6 THz (right).

When the x -polarized incident wave is proposed for RHS, the electric field diagrams of transmitted polarizer are shown in Fig. 7. The electric field diagrams of the polarizer without graphene strips in Fig. 7 (a). The area where the field strength is enhanced varies with different frequencies. When a graphene strip at E_F of 0.1 eV is loaded in Fig. 7 (b), the field strength focusing phenomenon at the corresponding frequency point is more obvious. The electromagnetic field accumulation in space among the tips of RHS resonator patches showing the capacitance characteristic. Via changing the Fermi energy, the impedance of the graphene strip is adjusted, and the metasurface structure parameters are adjusted. With the Fermi level of raise the permittivity of graphene gets closer and closer to the characteristics of gold. By optimizing various parameters, the proposed RHS of the original structure satisfies the condition of linear polarization conversion, that is, the amplitude of the transmitted y -polarized component equivalent to

the incident wave. Meanwhile, the phase difference is $\pm\pi+2k\pi$ approximately.

In order to analyze the performance of the RHS with graphene polarizer we designed, the transmittance of cross-polarization was simulated with x -polarized normal incidence are given in Fig. 8, while $E_F=\mu_c$ covers among 0.05eV and 1.0eV. It can be obtained that the transmitted terahertz waves are linearly polarized waves, when its phase difference $\Delta\varphi$ is given in Fig. 8 (a). The Figs. 8 (b), and (c) present the transmittance cross-polarized waves, the opposite propagation t_{xx} and absorption of the polarizer at different chemical potential μ_c . We plot the curve with the gradual increase of μ_c , the absorption rate of the transmitting polarizer continues to decrease, while the transmission cross-polarized wave gradually increases. When μ_c keeps increasing, the opposite propagation t_{xx} increases by a resonance point, so the frequency of the PCR is also broadened.

Figure 8 (d) shows the PCR simulation curves of graphene polarizer with different fermi energies. It can be seen from the figure $E_F=\mu_c=0.05\text{eV}$, 0.1V, 0.15eV, 0.2V, 0.25eV, 0.3eV, 0.5eV and 1 eV. The PCR of the proposed RHS are greater than 90% from 0.5 THz to 2.75THz. With the increase of E_F , the bandwidth is broadened, especially when $E_F=\mu_c=0.5\text{eV}$ and 1.0eV, the conversion rate reaches up to 99%. While it's transmitting polarization conversion efficiency maintains high performance. Therefore, it is concluded that the characteristics of the graphene strip are the key factor for the enhancement of the bandwidth of the proposed RHS polarizer.

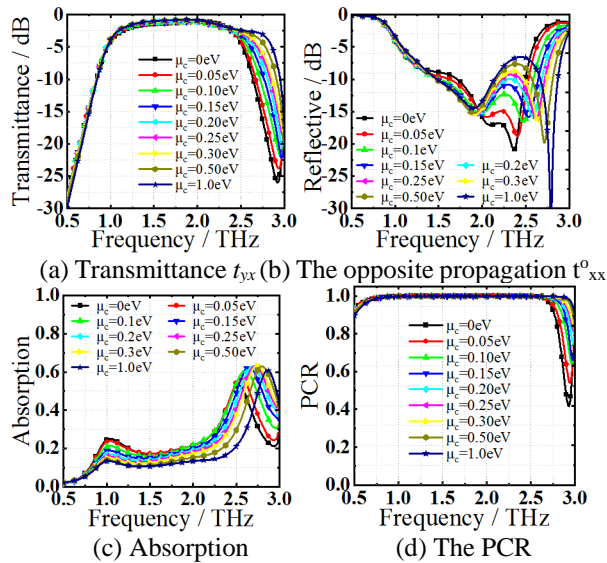


Fig. 8. The transmittance of cross-polarization was simulated vertical incidence with varying chemical potential $E_F=\mu_c$. (a) Transmittance cross-polarized waves t_{yx} , (b) transmissive co-polarized waves t_{xx} , (c) absorption, and (d) the PCR.

Finally, the transmittance of cross-polarization was simulated with x -polarized incidence at oblique incidence θ . As shown in Fig. 9 (a) with chemical potential $E_F=\mu_c=0.1\text{eV}$. From 1THz to 2THz, the high transmission performance can be maintained in the range of 0° - 60° with oblique incidence. The cross-polarization transmission performance in the high frequency range (2.1THz to 2.5THz) decreases when the oblique incidence is 60 degrees. In Fig. 9 (b), the opposite propagation t_{xx} gradually deteriorates and is greater than -10dB with the increase of oblique incident. In Fig. 9 (c), that it is mainly caused by the loss of absorption. The cross-polarized waves can transmit through the back of gratings, which still equivalent to a metal ground blocking the opposite propagation t_{xx} . The absorption rate of the polarizer is kept below 30% as the angle of incidence increases from 0.5 THz to 2 THz. Due to the metasurface structure of the device and graphene, as the incident angle increases, the absorption rate increases sharply from 2THz to 3THz. In Fig. 9 (d), from 0.5THz to 2.75 THz, the conversion rate is greater than 90%. The widening of the frequency is caused by the peaks in the PCR curve near 2.25, 2.75 and 2.9 THz. At these peaks, the efficiency is mainly limited by the dielectric loss.

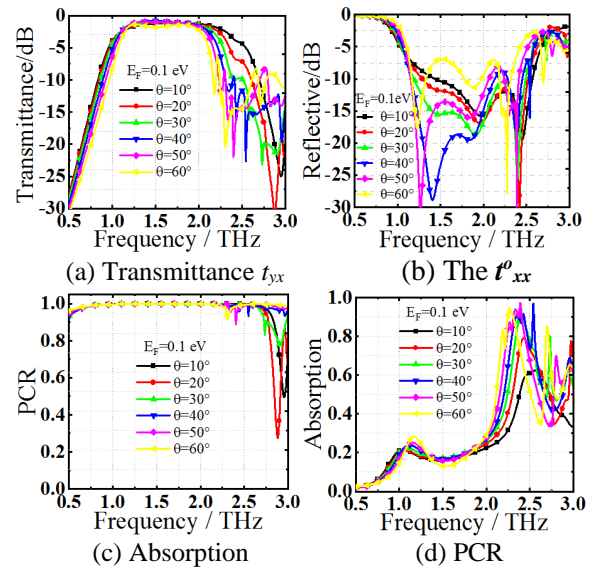


Fig. 9. The transmittance of cross-polarization was simulated or x -polarized incidence at oblique incidence θ with chemical potential $E_F=\mu_c=0.1\text{eV}$. (a) Transmittance cross-polarized wave's t_{yx} , (b) the opposite propagation t_{xx} , (c) absorption, and (d) PCR.

Compared with the other references in Table 2, the tri-layered resonant structure transmitting polarizer loaded with graphene is very competitive. The device achieves tunable ultra-wideband transmission performance. It is important that the PCR is still above 90% at large incident angles.

Table 2: Comparison of transmission polarizer performance

Ref.	OB (THz)	RB (PCR≥90%)	Tunable	OI
[17]	0.55-1.37	85.4%	No	0-45°
[18]	0.22-1.22	133%	No	No
[28]	0.23-1.17	134.3%	No	No
[29]	1.3-1.63	22.5%	Yes	0-90°
[30]	0.2-1.97	163.3	No	0-30°
This work	0.5-3	142.9%	Yes	0-60°

OB: Operator Bandwidth; RB: Relative Bandwidth; OI: Oblique incidence.

V. CONCLUSION

Our transmitting polarizers of graphene-based are wide incidence angle which achieved broadband and almost perfect polarization conversion transmission. In this study, two polarizers in the form of graphene strips are analyzed. The graphene strip of type B is on the diagonal of the unit structure, which has a high-performance over a broadband. Next, the performance of the graphene-based Type B polarizer was analyzed in detail, when E_F spans from 0.05eV to 1.0 eV. As the E_F increase, the bandwidth is also broadened, while its transmittance maintains high performance. Between 0.5 THz and 3 THz the PCR is greater than 90%, and the relative bandwidth up to 142.9%. Finally, the transmittance of cross-polarization was simulated at oblique incidence θ with chemical potential 0.1eV. The proposed novel tunable polarizer has high transmittance among in 0°-60°. The future research is the composite electromagnetic target simulation of the CATR, which is applied to the RF/THz composite scene simulation to cope with the complex and changing detection condition.

ACKNOWLEDGMENT

This research was supported by National Natural Science Foundation of China (Grant No. 61761012, 61661011), by Innovation Project of Guangxi Graduate Education (Grant No. YCBZ2019051), and by Guangxi Innovation Driven Development Special Fund Project (Grant No. GUIKEAA19254012).

REFERENCES

[1] N. K. Grady, J. E. Heyes, D. R. Chowdhury, Y. Zeng, M. T. Reiten, A. K. Azad, A. J. Taylor, D. A. R. Dalvit, and H.-T. Chen, "Terahertz metamaterials for linear polarization conversion and anomalous refraction," *Science*, vol. 340, pp. 1304-1307, 2013.

[2] A. Vakil and N. Engheta, "Transformation optics using graphene," *Science*, vol. 332, pp. 1291-1294, 2011.

[3] L. Zakrajsek, E. Einarsson, N. Thawdar, M. Medley, and J. M. Jornet, "Lithographically defined plasmonic graphene antennas for terahertz-

band communication," *IEEE Antennas and Wireless Propagation Letters*, vol. 15, pp. 1553-1556, 2016.

[4] M. I. Shalaev, J. Sun, A. Tsukernik, A. Pandey, and K. Nikolskiy, "High-efficiency all-dielectric metasurfaces for ultracompact beam manipulation in transmission mode," *Nano Letters*, vol. 15, pp. 6261-6266, 2015.

[5] M. Camacho, M. Camacho, R. R. Boix, S. A. Kuznetsov, M. Beruete, and M. Navarro-Cía, "Far-field and near-field physics of extraordinary THz transmitting hole-array antennas," *IEEE Transactions on Antennas and Propagation*, vol. 67, pp. 6029-6038, 2019.

[6] M. Chen, L. Chang, X. Gao, H. Chen, C. Wang, X. Xiao, and D. Zhao, "Wideband tunable cross polarization converter based on a graphene metasurface with a hollow-carved "H" array," *IEEE Photon. J.*, vol. 9, pp. 1-11, 2017.

[7] B. Vasic, D. C. Zografopoulos, and G. Isic, "Electrically tunable terahertz polarization converter based on overcoupled metal-isolator-metal metamaterials infiltrated with liquid crystals," *Nanotechnology*, vol. 28, p. 124002, 2017.

[8] A. Zubair, D. Tsentalovich, C. Young, M. Heimbeck, and J. Kono, "Carbon nanotube fiber terahertz polarizer," *Applied Physics Letters*, vol. 108, no. 14, p. 141107, 2016.

[9] D. J. Liu, Z. Y. Xiao, X. L. Ma, K. K. Xu, J. Y. Tang, and Z. H. Wang, "Broadband asymmetric transmission and polarization conversion of a linearly polarized wave based on chiral metamaterial in terahertz region," *Wave Motion*, vol. 66, pp. 1-9, 2016.

[10] X. Yu, X. Gao, W. Qiao, L. Wen, and W. Yang, "Broadband tunable polarization converter realized by graphene-based metamaterial," *IEEE Photonics Technology Letters*, vol. 28, 1-1, 2016.

[11] X. Gao, W. Yang, W. Cao, M. Chen, and H. Li, "Bandwidth broadening of a graphene-based circular polarization converter by phase compensation," *Opt. Express*, vol. 25, pp. 23945-23954, 2017.

[12] L. Peng, X. Li, X. Jiang, and S. Li, "A novel THz half-wave polarization converter for cross-polarization conversions of both linear and circular polarizations and polarization conversion ratio regulating by graphene," *Journal of Lightwave Technology*, vol. 36, pp. 4250-4258, 2018.

[13] F. Fan, S. Xu, X. Wang, and S. Chang, "Terahertz polarization converter and one-way transmission based on double-layer magneto-plasmonics of magnetized InSb," *Optics Express*, vol. 24, no. 23, pp. 26431-26443, 2016.

[14] J. Woo, S. Hussain, and J. Jang, "A terahertz in-line polarization converter based on through-via connected double layer slot structures," *Scientific Reports*, vol. 7, p. 42952, 2017.

- [15] H. Mao, L. Xia, X. Rao, H. Cui, S. Wang, Y. Deng, D. Wei, J. Shen, H. Xu, and C. Du, "A terahertz polarizer based on multilayer metal grating filled in polyimide film," *IEEE Photonics Journal*, vol. 8, pp. 1-6, 2017.
- [16] J. Su, Z. Li, Z. Li, Q. Guo, and Y. Yang, "Ku-band phase-gradient metasurface for broadband high-gain circularly polarized lens antenna," *Applied Computational Electromagnetics Society Journal*, vol. 34, no. 5, pp. 669-675, 2019.
- [17] X. Jing, X. Gui, P. Zhou, and Z. Hong, "Physical explanation of Fabry-Pérot cavity for broadband bilayer metamaterials polarization converter," *Journal of Lightwave Technology*, vol. 36, pp. 2322-2327, 2018.
- [18] R. T. Ako, W. S. L. Lee, S. Atakaramians, M. Bhaskaran, and W. Withayachumnankul, "Ultra-wideband tri-layer transmissive linear polarization converter for terahertz waves," *APL Photonics*, vol. 5, no. 4, pp. 0461011-0461017, 2020.
- [19] S. Masuminia, C. Ghobadi, J. Nourinia, M. Karamirad, and B. Mohammadi, "A novel tunable graphene based terahertz absorber with polarization insensitive," *Applied Computational Electromagnetics Society Journal*, vol. 31, no. 12, 1439-1444, 2016.
- [20] K. Xu, J. Li, A. Zhang, and Q. Chen, "Tunable multi-band terahertz absorber using single-layer square graphene ring structure with T-shaped graphene strips," *Optics Express*, vol. 28, no. 8, 2020.
- [21] S. Xia, Z. Xiang, H. Yu, J. Liu, L. Wang, and S. Wen, "Graphene surface plasmons with dielectric metasurfaces," *Journal of Lightwave Technology*, vol. 35, pp. 4553-4558, 2017.
- [22] Y. Gang, F. Ling, Y. Jin, and Y. Rao, "Dynamically tunable terahertz cross polarization amplitude based on graphene metamaterials," *Optoelectronic Devices & Integration*, 38, JW3A, 2015.
- [23] X. Li, L. Lin, L. Wu, W. Yin, and J. Mao, "A, bandpass graphene frequency selective surface with tunable polarization rotation for THz applications," *IEEE Transactions on Antennas and Propagation*, vol. 65, pp. 662-672, 2017.
- [24] X. He, A. Hu, and X. Guo, "In-fiber graphene-h-BN polarizer with enhanced performance and bandwidth," *IEEE Photonics Journal*, vol. 99, 1-1, 2019.
- [25] S. Amanatiadis, T. Ohtani, Y. Kanai, and N. Kantartzis, "Effective design of graphene patch arrays for adjustable plane-wave scattering," *Applied Computational Electromagnetics Society Journal*, vol. 35, no. 11, pp. 1310-1311, 2021.
- [26] D. Chen, Y. Li, and X. Pang, "MMW/IR beam combiner with graphene IR window for MMW/IR compact range compound test," *Appl. Phys. Lett.*, vol. 110, p. 251902, 2017.
- [27] G. W. Hanson, "Dyadic, Green's functions for an anisotropic, non-local model of biased graphene," *IEEE Trans. Antennas Propag.*, vol. 56, pp. 747-757, 2008.
- [28] Y. Cheng, R. Gong, and L. Wu, "Ultra-broadband linear polarization conversion via diode-like asymmetric transmission with composite metamaterial for terahertz waves," *Plasmonics*, vol. 12, pp. 1113-1120, 2017.
- [29] L. Dai, Y. Zhang, Y. Zhang, S. Liu, and H. Zhang, "Multifunction tunable broadband terahertz device for polarization rotation and linear asymmetric transmission based on Dirac semimetals," *Optics Communications*, vol. 468, p. 125802, 2020.
- [30] W. Pan, Q. Chen, Y. Ma, X. Wang, and X. Ren, "Design and analysis of a broadband terahertz polarization converter with significant asymmetric transmission enhancement," *Optics Communications*, vol. 459, p. 124901, 2019.